Catalysis Today 150 (2010) 91–99

Contents lists available at ScienceDirect

Catalysis Today

journal homepage: www.elsevier.com/locate/cattod

Synthesis of carbon monolith with bimodal meso/macroscopic pore structure and its application in asymmetric catalysis

Yong-Suk Kim, Xiao-Feng Guo, Geon-Joong Kim *

Department of Chemical Engineering, Inha University, 253 Younghyun-dong, Incheon, Nam-gu 402-751, Democratic People's Republic of Korea

ARTICLE INFO

Article history:
Available online 17 October 2009

Keywords:
Bimodal pores
Mesoporous carbon monolith
SBA-15
Enantioselective catalysis

ABSTRACT

Carbon monolith with bimodal meso/macroporous pore structures was synthesized by the nanocasting method, using corresponding monolith silica as templates. The pore system of this material was characterized by instrumental analysis. The adjacent macropores are interconnected through uniform-sized windows, and the walls of macrospheres consist of mesostructured pores. Chiral Co(III)-(BF_3) salen immobilized on a meso/macroporous carbon monolith can be applied as an effective heterogeneous catalyst for an asymmetric reaction such as a hydrolytic kinetic reaction of terminal epoxides. The catalysts were prepared with different loading amounts of aluminium chloride to anchor the active salen complex, and the catalytic activity increased with increasing amount of aluminum chloride on the surfaces, showing up to 99 ee% of the product epichlorohydrin (ECH).

1. Introduction

For a variety of applications, it would be advantageous to have material with pores in two or three different length scales in an ordered fashion, with a hierarchical structure and interconnectivity between the pores. For catalytic applications, reactant molecules need to readily access the interior pore structure. Hierarchical materials containing both interconnected macroporous and mesoporous structures have enhanced properties compared with single-sized pore materials, due to increased mass transport through the pore channels with a high specific surface area at the molecular level.

Porous carbons fabricated by the nanocasting method, using inorganic silicas as a mold, have attracted wide interest during the past decade [1–11]. These carbons, characterized by high specific surface area, uniform textural pores, and large pore volume, have been applied in many areas including catalysis, separation, and adsorption and energy storage [12,13]. Most carbons are generally produced as a powder form in the size range from 1 to 10 μm. However, under certain circumstances, the powder-like morphology makes it difficult to use the material as is. For example, as an electrode of a double layer capacitor, carbon powders must be glued to form a flat layer. When used as a separation or adsorption media, the fine carbon powders packed into a column may bring high back-pressure. One possible way to solve these problems is to fabricate the carbon materials directly into a monolithic shape. Recently, several groups have reported the successful synthesis of monolithic carbons by nanocasting different templates, including silica monoliths [14–18], particle arrays [19,20], and polymer foams [21,22]. By selecting the proper templates, the morphology and pore structure of the final carbon monoliths can be easily controlled to cater to various applications. To date, two kinds of carbon monoliths, with different porous structures, have been fabricated. Zhao and Mokaya et al. have utilized ordered mesoporous silica aggregates, via chemical vapor deposition or polymerization followed by carbonization, to prepare carbon monoliths [15,16]. The as-obtained carbon monoliths feature a high surface area and exclusively mesoporous structure, but in most cases, these materials do not have much practical value because the interior of the carbons is not easily accessible [21,22]. Recently, some groups have reported carbon monoliths with a hierarchical macro/mesoporous structure [17,18,21,22]. The presence of large macropores (also through-pores or perfusion-pores) facilitates the rapid transport of species to the interior of monoliths, whereas mesopores guarantee a large surface area for interaction. The well-arranged, open porous structure of this kind of carbon monolith renders it very useful for a variety of purposes. Further, different macroscopic morphologies are needed for advanced property research. Meso/macroporous carbon monolith with a highly ordered pore size is an especially ideal material for an electrochemical doubly layered capacitor (EDLC) as well as catalysis. But so far, high-ordered meso/macroporous carbon monoliths with three-dimensional (3D) structure using meso/macroporous silica as a hard template, which would be ideal for these purposes, have not been reported.

* Corresponding author. Fax: +82 32 872 4046.
E-mail address: kimgj@inha.ac.kr (G.-J. Kim).

0920-5861/$ – see front matter © 2009 Elsevier B.V. All rights reserved.
doi:10.1016/j.cattod.2009.09.005

In the present work, we report a new carbon monolith with bimodal meso/macroporous 3D structure. A simple and versatile procedure, by coupling nanocasting and phase separation, was proposed for its synthesis. This carbon monolith, having novel pore structure with macroporous skeletons and mesoporous walls, was employed as an efficient support to immobilize active salen complexes for asymmetric catalysis. In this work, trends in activity and enantioselectivity of chiral Co(III)-BF_3 salen immobilized on meso/macroporous carbon composites have been examined in a hydrolytic kinetic resolution (HKR) of epoxide. These catalysts exhibited very high activity and selectivity to form an optically pure epoxide, with up to 99 ee%.

2. Experimental

2.1. Synthesis of meso/macroporous silica template and mesoporous carbon monolith

2.1.1. Synthesis of meso/macroporous SBA-15 or -16 silica monolith

The meso/macroporous composites were synthesized from the mixture of two types of prehydrolyzed silica sol (SBA-15 and SBA-16) and PMMA polymer spheres. The typical synthetic procedure for the mesoporous SBA-15 sol is as follows: first, the calculated amount of poly(ethylene oxide)-*block*-poly(propylene oxide)-*block*-(ethylene oxide) (EO_{20} PO_{70} EO_{20}) (P-123); numbers in subscripts denote the molar ratios of each component) was dissolved in EtOH to make 35 wt% solution. To prepare the prehydrolyzed precursor solution, tetraethyl orthosilicate (TEOS) was dissolved in EtOH solution acidified by aqueous hydrochloric acid (HCl). After mixing the two solutions, the mixture was refluxed for 8 h, and then the solvent was partially evaporated. The initial molar ratio of TEOS:EtOH:H_2O:HCl was 1:3:4:0.04.

In a typical preparation of SBA-16 sol, 2.0 g of (ethylene oxide)$_{106}$–(propylene oxide)$_{70}$–(ethylene oxide)$_{106}$ (Pluronic F-127) was dissolved in the solution of EtOH(4.69 g), H_2O(0.94 g) and 2M-HCl(0.15 g) while stirring at 298 K. Into that solution, 6.25 g of TEOS was added slowly while stirring at 308 K for 1 h. The mixture was aged at 353 K for 2 h without stirring to evaporate the solvent, until the viscous solution was recovered. Monodispersed PMMA spheres with a diameter of 30 μm (TAFTIC$_{TM}$ FH-S series; for use with a light diffuser) were purchased from Toyobo Co. The SBA-15 or SBA-16 silica sol solution made by sol–gel process was added to the same volume of PMMA spheres. The whole mixture was stirred at room temperature, and then centrifuged in a polypropylene tube with 13,000 rpm. Then the mixture was dried slowly at room temperature for 5 days. The PMMA spheres were removed by direct calcination at 873 K for 4 h in air. The heating rate was maintained at 1 K/min.

2.1.2. Synthesis of meso/macroporous carbon monolith

The anhydrous 1.0 M-$ZnCl_2$ solution in ethylether was incorporated into the pores of calcined meso/macroporous silica monolith for two times. $ZnCl_2$ was impregnated on the surfaces of silica after evaporation of ether to generate the catalytic sites for the polymerization of fulfuryl alcohol. The polymerization was carried out by heating the $ZnCl_2$-impregnated silica in fulfuryl alcohol at 333 K for 3 h. The resulting solid sample was dried at 398 K for 12 h after washing the outer surfaces with ethanol. The silica/resin composites were heated under a nitrogen atmosphere at the heating rate of 5 K/min to 1173 K, and held at this temperature for 7 h to carbonize the polymer inside the mesopores of SBA type silica. The carbon–silica composite obtained after pyrolysis was treated with 5 wt% hydrofluoric acid at room temperature to remove the silica template. The template-free carbon product was filtered, washed with ethanol, and dried at 393 K. The meso/macroporous carbon monolith will be denoted as C-SBA-15 and C-SBA-16, respectively.

2.1.3. Surface oxidation of meso/macroporous carbon monolith

As-synthesized meso/macroporous carbon monolith (C-SBA-15 or C-SBA-16; 0.2 g) and 100 mL methylene chloride (MC) were added to a 250 mL flask, and the suspension was vibrated ultrasonically for 0.5 h. After addition of phase transfer agent tetrabutylammonium bromide (TBABr, TCI Co.; 1.0 g) dissolved in the mixed solution of H_2O (10 mL) and acetic acid (10 mL), as well as an aqueous solution of potassium permanganate (5.0 g; dissolved in 5 mL H_2O), the mixture was stirred vigorously at 298 K for 24 h. The powder was washed with aqueous HCl and methanol. The washing with methanol was repeated at least four times. The sample was dried in a vacuum oven overnight at 338 K.

2.1.4. Immobilization of chiral salen catalyst on the bimodal porous materials

The anhydrous aluminum chloride was immobilized on the ordered mesoporous carbon monolith in order to anchor the chiral salen complex as an active site for the enantioselective catalyst. Aluminum chloride was dissolved in dried tetrahydrofuran (THF), and the meso/macroporous carbon monolith having the oxidized surfaces (or silica SBA-16) was added to that solution. The loading amount of aluminum chloride was controlled from 10 wt% to 30 wt% (Al basis) to the functionalized meso/macroporous carbon monolith support. After evaporation of solvent, the recovered solid sample was calcined at 823 K for 2 h under nitrogen.

The chiral Co(III)-(BF_3) salen was prepared by the same method as shown in the previous paper [23]. The structure of chiral Co(III)-(BF_3) salen is indicated in Scheme 1. The Al-containing mesoporous C-SBA-16 or SBA-16 silica was used as a support for immobilization of chiral (salen) cobalt complexes. The procedure to anchor the chiral complexes on the surfaces of meso/macroporous C-SBA-16 is also shown in Scheme 1. The heterogenized chiral salen catalysts were prepared by refluxing Al-containing mesoporous C-SBA-16 monolith with the solution containing the chiral Co(III)-(BF_3) salen complex in MC for 2 h. The sample, with a dark green color, was obtained by filtration and sequential washing with MC, THF and methanol until the filtrate was colorless. The catalyst was dried in vacuo to yield a heterogenized Co (salen) complex.

2.1.5. General procedure for the catalytic reaction

In a representative reaction between epichlorohydrin (2-(chloromethyl)oxirane; ECH) and water, the catalyst (1.0 mol% salen-loading relative to ECH/support), THF solvent (5 mL) and (±)-ECH (0.93 g, 10 mmol) were charged in an oven-dried 25 mL flask and the reaction mixture was stirred in open atmosphere at ambient temperature. After addition of water (81 mg, 4.5 mmol), the resultant mixture was stirred for 40 h, and enantiomeric excess percentage (ee%) values of the ring-opened product were determined by GC using a chiral capillary column (CHIRALDEX, γ-cyclodextrin trifluoroacetyl, 20 m × 0.25 mm i.d.), and by HPLC using a Chiralcel® OD-H column (24 cm × 0.46 cm).

2.1.6. Characterization

X-ray powder diffraction (XRD) data were acquired on a D/MAX 2500 V/PC diffractometer using Cu Kα radiation. The data were collected from 0.6 to 3° (2θ) with a resolution of 0.02°. The morphology and microstructures of as-prepared samples were characterized by field emission transmission electron microscopy operating at 200 kV (FE-TEM, S-4200). The morphology and size of macropores were determined by scanning electron microscopy (SEM) with a Hitachi S-4200 microscope. SEM-EDX was used to analyze the anchored cobalt contents. Nitrogen adsorption and desorption isotherms were measured at 77 K using a micromeritics

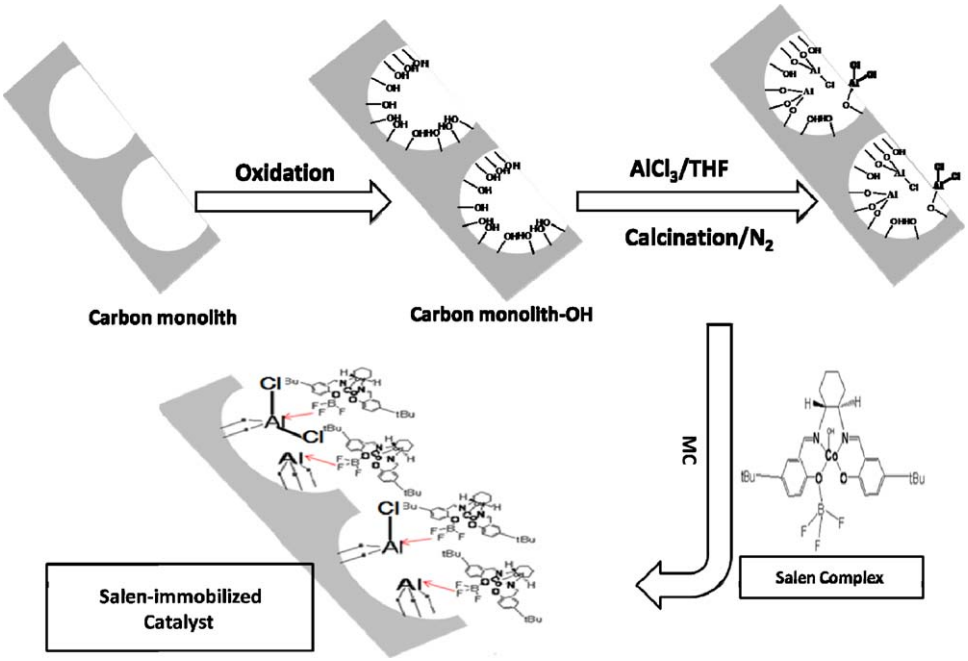

Scheme 1. Schematic illustration of Co (III) salen complexes immobilized onto the functionalized meso/marcoporous carbon monolith.

ASAP 2010 system. The data were analyzed using the Brunauer–Emmett–Teller (BET) model. Both adsorption and desorption branches were used to calculate the pore size distribution by the Barrett–Joyner–Halenda method. The pore volumes were taken at the $P/P_0 = 0.995$ single point. The specific surface areas were calculated according to BET theory. The dispersivity of carbon monolith and functionalized carbon monolith in methanol solvent was tested by a Turbiscan analyzer (Fomulation Turbiscan Lab).

Fig. 1. Photographs of the silica SBA-15 (A); carbon monolith C-SBA-15 (B); silica monolith SBA-16 (C); carbon C-SBA-16 (D).

The coordination of Al on the C-SBA-16 and silica SBA-16 was characterized by ^{27}Al-MAS NMR spectroscopy (DSX 400 MHz Solid State Bruker NMR(at KBSI Daegu); 400 MHz with magic angle spinning at 10 kHz, $\pi/2$ pulse, 2 μs contact time, a repetition delay of 2 s and 30,000 scans).

3. Results and discussion

3.1. Characterization of meso/macroporous monoliths

The centimeter-scale silica monoliths were synthesized by using the corresponding SBA-15 or SBA-16 sol and PMMA template to control the bulk shape and macropore structure. The particle size distribution of PMMA was very narrow, and the particles were spherical in shape with a uniform size of around 30 μm. In this case, the silica sol filled the void volume between the cross-packed PMMA spheres. The SBA-15 or SBA-16 silica sol was solidified after removal of solvents to form the monolith structure (Fig. 1). The shape of the meso/macroporous silica monolith appears to replicate the centrifuge tube shape, as shown in Fig. 1. In addition, the size of the macroporous channels could be controlled by changing the size of the template polymer spheres. During the calcinations to remove the PMMA templates, densification of the silica network occurred, resulting in shrinkage of the monolith.

Nanocasting by using two- or three-dimensional (2D or 3D) structured mesoporous silica as a mold was applied to fabricate the C-SBA-15 or C-SBA-16 monolith. The apparent morphologies of those meso/macroporous carbon monoliths were replicated by the corresponding meso/macroporous silica monolith template, as shown in Fig. 1. The silica sol became a white solid monolith having the same shape as the molding container, whereas mesoporous C-SBA-15 and C-SBA-16 monolith are black in color, maintaining the shape of the silica templates. However, large and moldable meso/macroporous carbon monolith could be obtained successfully in centimeter scale, maintaining the same shape of container. Obvious shrinkage in volume was observed after carbonization.

Scanning electron microscope (SEM) images of as-synthesized silica and carbon monoliths are shown in Fig. 2. As-synthesized silica monolith (SBA-15) shows a uniform macropore size of 30 μm and a highly ordered 3D well-interconnected network through macroporous windows. It can be seen that large fractions of the calcined sample were highly ordered in three dimensions and the remaining portions exhibited uniform macroporosity interconnected through windows whose diameter is typically the same as that of the PMMA template used. In C-SBA-15 sample, a 3D well-interconnected network was formed with an average macropore channel size of 30 μm (Fig. 2B). As-synthesized silica monolith (SBA-16) also shows the highly ordered macropore channels interconnected 3-dimensionally through windows, similar to the structure of silica monolith (SBA-15). It was observed that carbon monolith C-SBA-16 has a much thicker wall than C-SBA-15.

Evidence of ordered mesopores in the meso/macroporous silica monolith was found by XRD, TEM and N_2 adsorption/desorption analysis. For studying the interior structures and the morphology of silica and carbon monoliths, samples were further analyzed by TEM. Silica monolith SBA-15 and -16 samples prepared in this study had the ordered mesoporous pore inside the macroporous walls (Fig. 3A and C). The C-SBA-15 and C-SBA-16 monolith

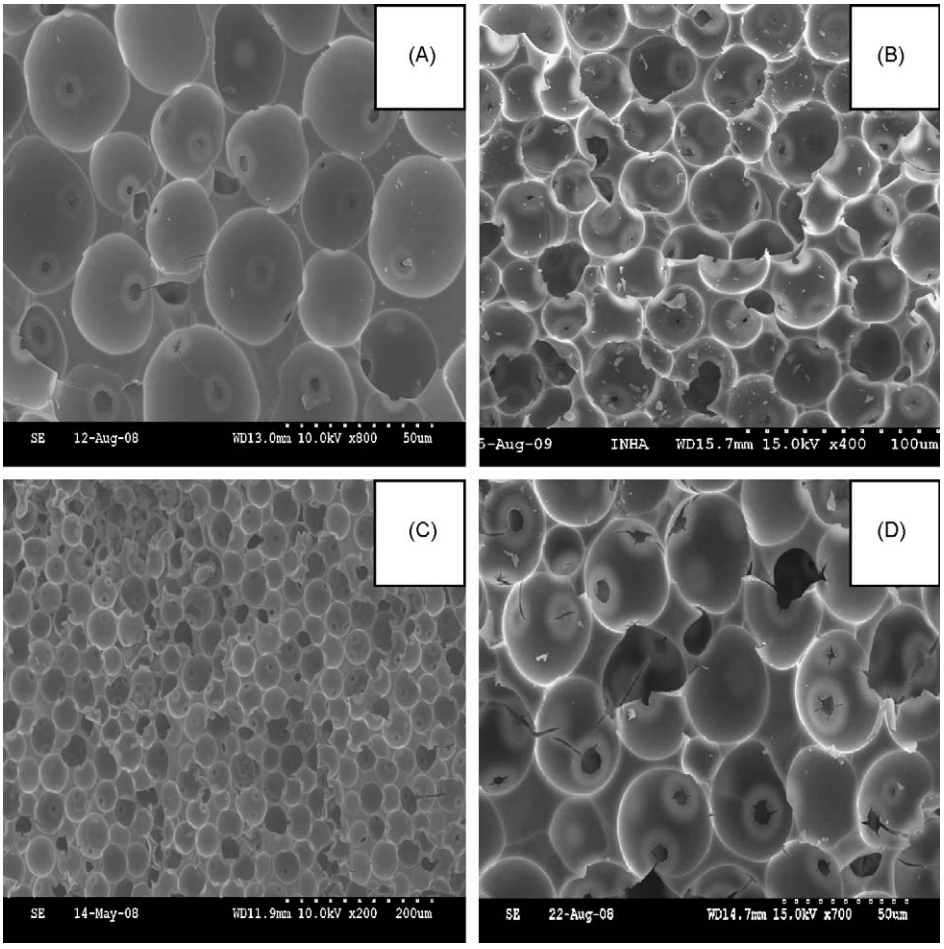

Fig. 2. SEM images of the silica monolith SBA-15 (A); carbon monolith C-SBA-15 (B); silica monolith SBA-16 (C); C-SBA-16 (D).

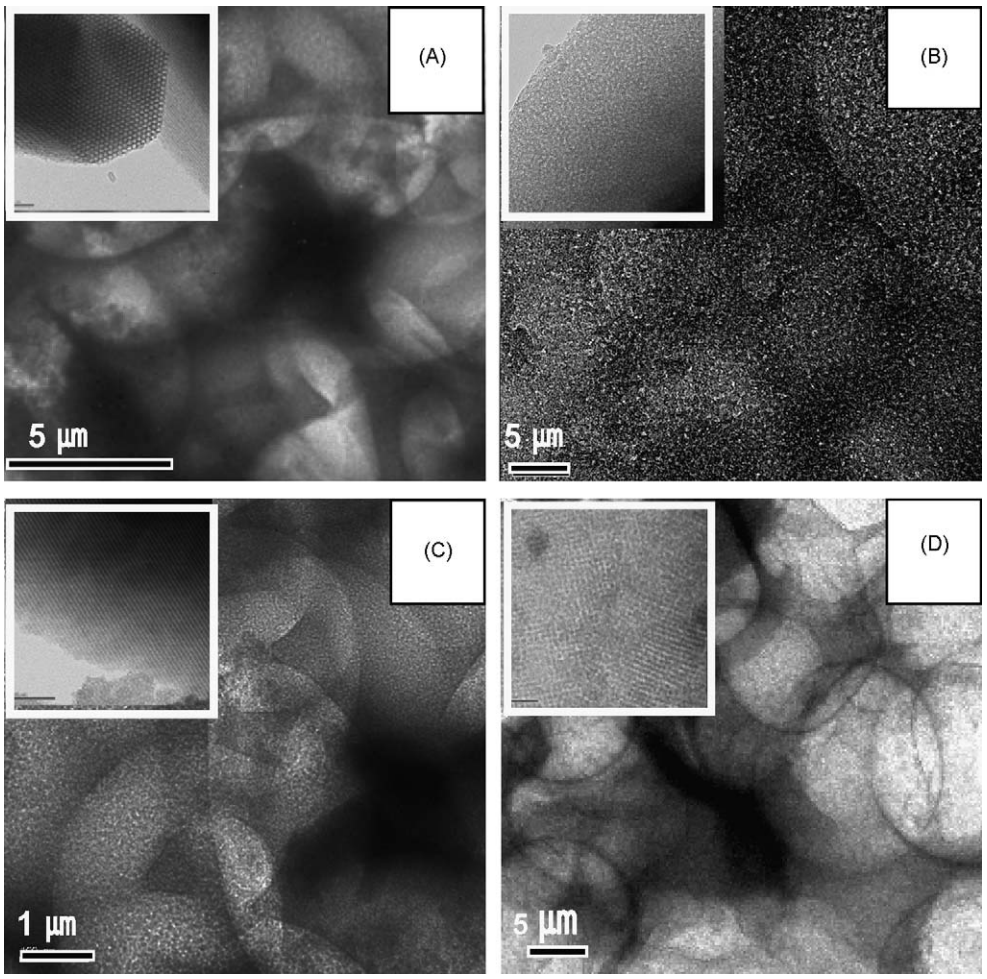

Fig. 3. TEM images of the silica SBA-15 (A); carbon monolith C-SBA-15 (B); silica SBA-16 (C); and carbon monolith C-SBA-16 (D).

showed partly disordered mesopores distributed inside the wall of the macropores (Fig. 3B and D). Silica monolith SBA-16 as well as C-SBA-16 showed mesoporosity throughout the whole of the SBA-16 matrix. As can be seen in Fig. 3, the overlapped void volume of spherical macropores and also the mesopores in the silica or carbon walls are visible in TEM images. An array of interconnected macropore structures over a large area provides more openings of porous channels.

Fig. 4 shows the X-ray diffraction patterns of silica SBA-15, SBA-16 made by the sol–gel process, and carbon monoliths C-SBA-15 and C-SBA-16 fabricated by the nanocasting method. In Fig. 4, SBA-15 silica shows a very intense (1 0 0) diffraction peak with additional three weak (1 1 0, 2 0 0, and 2 1 0) peaks after calcination, indicating the well-developed 2D hexagonal pore structure. The meso/macroporous carbon monolith C-SBA-15 showed a similar XRD pattern to that of silica SBA-15, but the peak for (1 0 0) diffraction was shifted higher. This means that the pore size of carbon monolith C-SBA-15 was decreased as compared to that of its parent template SBA-15 silica. For determination of the mesopore structure and the symmetry of SBA-16, XRD analysis was performed, and the diffraction patterns of SBA-16 are shown in Fig. 4. The reflection patterns could be indexed to the structure of the mesopores. SBA-16 exhibited an intense (1 0 0) diffraction peak with a distinctive shoulder peak due to the (0 0 2) plane. In addition, the broad and unresolved peak for the (1 0 1) plane at 1.5° (2θ) from the sample of SBA-16 silica obtained from the sol was investigated, revealing the 3D hexagonal symmetry of its pore structures. In Fig. 4D, XRD patterns of the meso/macroporous

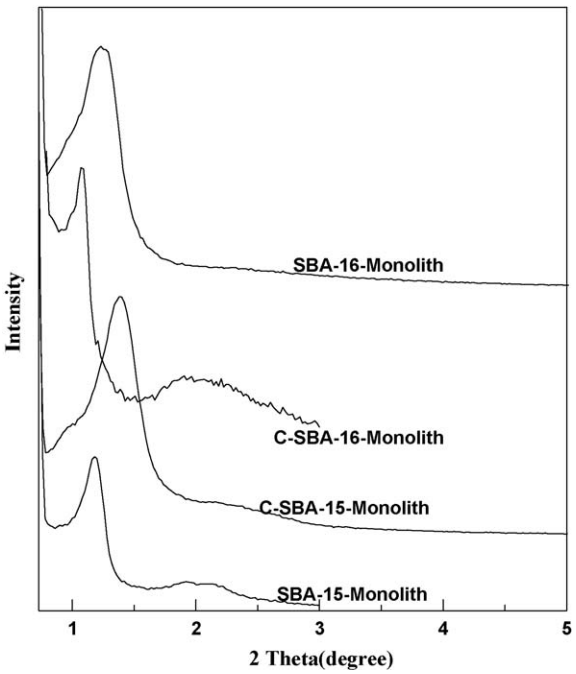

Fig. 4. X-ray diffractograms of silica monolith SBA-15, -16, carbon monolith C-SBA-15 and C-SBA-16.

Table 1
Pore structural parameters of meso/macroporous C-SBA-15 and -16 carbon monolite, as well as the parent silica template SBA-15 and -16.

Entry	Type of support	Specific surface area (m^2/g)	Pore volume (cm^3/g)	Averaged pore size (Å)
1	Silica SBA-15	721	0.92	78.3
2	Silica SBA-16	650	0.98	62.0
3	Carbon SBA-15	851	1.17	66.0
4	Carbon SBA-16	901	1.24	75.6
5	10 wt% Al/carbon SBA-15	660	0.66	54.6
6	30 wt% Al/carbon SBA-15	666	0.62	48.0

carbon monolith C-SBA-16 are also listed, and this carbon replica obtained from SBA-16 silica monolith exhibited a diffraction pattern similar to the SBA-16 silica, showing the same pore structures.

The pore structural parameters of the parent SBA silica and their carbon replica materials are shown in Table 1. Large surface area, pore volumes, and pore sizes were formed in the meso/macroporous carbon composites. As can be seen in Table 1, it is clear that the mesoporosity of the carbon material was maintained after loading of 20 wt% $AlCl_3$ and calcination at 873 K in nitrogen, but it was partially blocked by Al compounds in the mesopore channels. The surface area, pore volume, and mean pore size were decreased after impregnation of aluminum sources.

The nitrogen physisorption isotherms for four types of monolith samples are plotted in Fig. 5. The isotherm of silica monolith SBA-15 (Fig. 5A) is of type IV according to IUPAC classification [24], having a typical H1 hysteresis loop for materials with hexagonal pore channels. The N_2 adsorption–desorption isotherm of calcined C-SBA-15 displays steep changes with increasing pressure, which is an indication of the presence of mesoporosity (Fig. 5C). In Fig. 5B, silica monolith SBA-16 indicated an ordered cage-like mesopore, showing the typical H2 type hysteresis. However, carbon monolith C-SBA-16 showed a combined hysteresis curve of H4 and H2.

To investigate the degree of functionalization of hydroxy groups, dispersion of parent carbon monolith and surface-oxidized carbon monolith C-SBA-15 was analyzed by Turbiscan using different solvents (water, methanol, and toluene). For this analysis, the monolith sample was ground into fine powders. The parent carbon monolith was aggregated, and settled down completely in water and toluene solvent. They exhibited good dispersal stability in methanol even after several weeks, indicating strong hydrophilicity of their surfaces. However, as-synthesized monolith aggregated completely even using methanol as solvent. Quantitative analysis using a novel optical analyzer (Turbiscan) was also employed to measure the dispersion stability of hydroxy-functionalized carbon monolith in water, toluene, and methanol. The interpretation of the transmission profiles was adopted to determine the dispersivity in the solvent by comparing the change in light transmission caused by the sedimentation of the carbon monolith in a sample cell. When sedimentation takes place in the suspension, the transmission profiles vary with the dispersed height of the sample with time. On the other hand, if the dispersion is stable, no discernible change in the transmission profile with time is observed over the entire sample cell. The aggregation and sedimentation behavior was monitored for each carbon sample, and the results of the transmission profile obtained in 15 min intervals are plotted as the transmission intensity versus time in Fig. 6.

3.2. Immobilization of chiral salen complexes

In this work, the homogeneous chiral Co(III)-BF_3 salen catalyst was chosen as a candidate to immobilize on the surfaces of Al-containing mesoporous C-SBA-15 or -16 monolith. UV, FT-IR, ESCA,

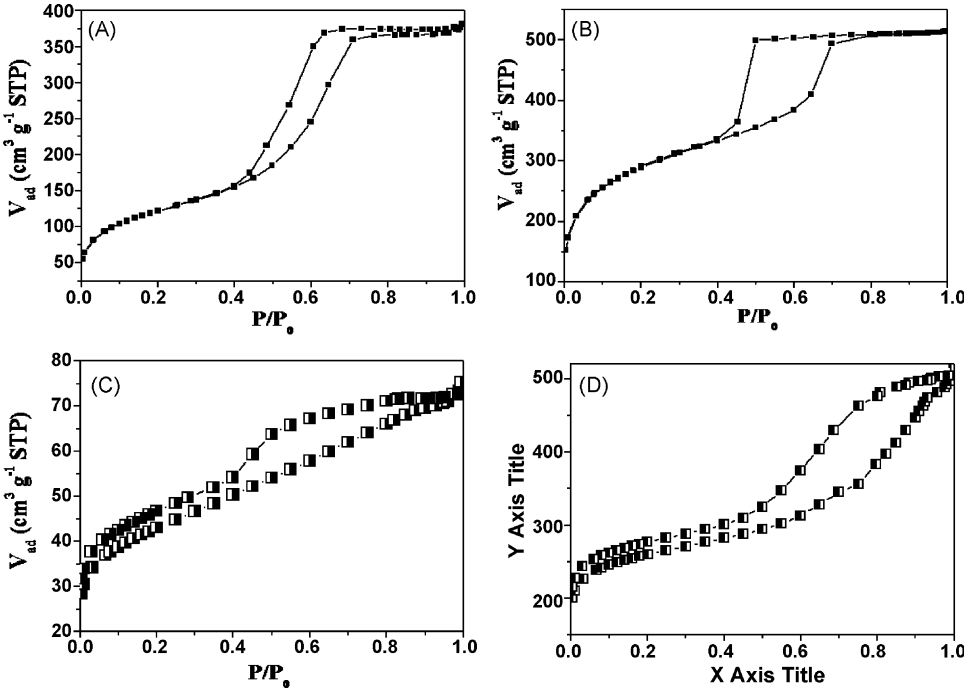

Fig. 5. N_2 adsorption–desorption isotherms of silica SBA-15 (A); silica SBA-16 (B); carbon monolith C-SBA-15 (C); and C-SBA-16 (D).

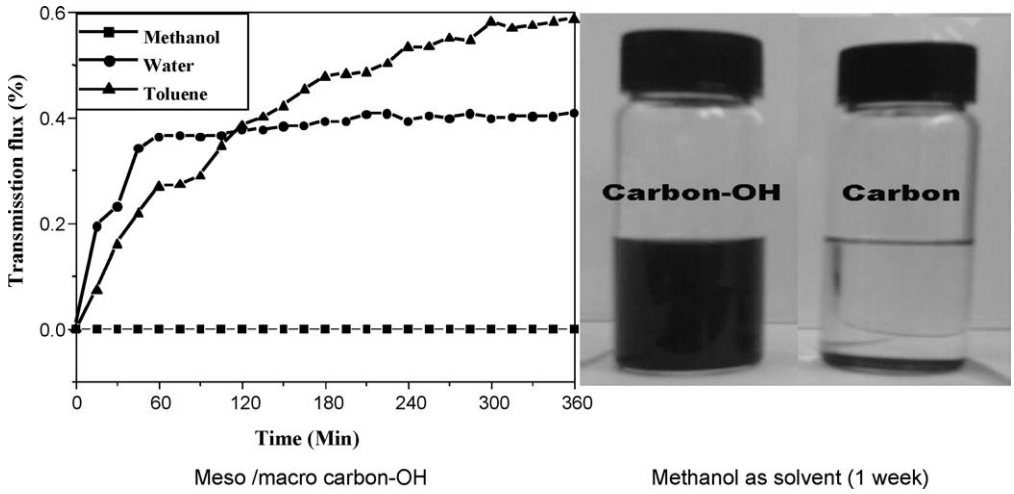

Fig. 6. Dispersion of parent carbon monolith and hydroxy-functionalized carbon monolith.

and NMR analyses were performed to determine the structure of the synthesized homogeneous cobalt-salen catalysts, and the results were reported previously [23]. These Co (salen) complexes were easily attached onto the acidic sites of supports, and they adhered strongly to the solid surfaces even after washing with various polar solvents. We believe this unique immobilization is due to the adsorption of the complex on to Lewis acid sites of aluminum present on the support, since the homogeneous Co(III)-BF_3 salen was also attached strongly to the surfaces of pure Al_2O_3. However, the Co(III)-salen having BF_3 group was easily attached onto the hydronium ions such as BrÖnsted acidic solids as reported in the paper. For instance, SiO_2–Al_2O_3 support having BrÖnsted acid sites mainly could immobilize the chiral Co(III)-BF_3 salen in a large amount.

To perform the immobilization of chiral Co(III)-BF_3 salen on the surfaces of carbons, anhydrous $AlCl_3$ was impregnated first on the carbons or SBA silica in the range of 10–30 wt%, and the dried sample was calcined at 550 °C in N_2 stream. In present work, ^{27}Al-MAS-NMR analysis was performed to distinguish the coordination state of aluminium compound which were formed after Al loading on the supports. Fig. 7 shows the ^{27}Al-MAS-NMR spectra of 30 wt% Al-incorporated SBA-16 silica and carbon samples with the different loading amounts. There are two distinct peaks on the ^{27}Al-MAS-NMR spectra of 30 wt% $AlCl_3$-loaded carbon (Fig. 7A). The strong peak at 0 ppm can be attributed to the octahedral coordination (Lewis acidic sites), and the chemical shift of 60 ppm is related to the aluminum atoms with tetrahedral coordination (BrÖnsted acidic sites). For the carbon sample containing 10 wt% $AlCl_3$ (Fig. 7B), only the Lewis acidic Al-sites appeared without the presence of BrÖnsted acid sites. When 30 wt% of $AlCl_3$ was impregnated on the SBA-16 silica, three distinct peaks on the ^{27}Al-MAS-NMR spectra were found as in Fig. 7C. The peak at chemical shift of 20 ppm in the spectrum is interpreted as 5-coordinated Al-site: namely these aluminums are surrounded by 4 oxygens in the framework with one adsorbed molecule such as water at the non-framework position [25]. There are many vacant tetrahedral sites and OH silanol groups on the surfaces of SBA-16 silica. In general, the silanol nest present on the surfaces of SBA-16 can be combined with aluminum species to form the tetrahedral sites or octahedral sites. The ^{27}Al-MAS-NMR spectra clearly showed that Lewis acidic sites were formed mainly on the surfaces of mesoporous carbon by attachment of $AlCl_3$. Higher concentration of BrÖnsted acidic sites was formed on the surfaces of SBA-16 silica than mesoporous

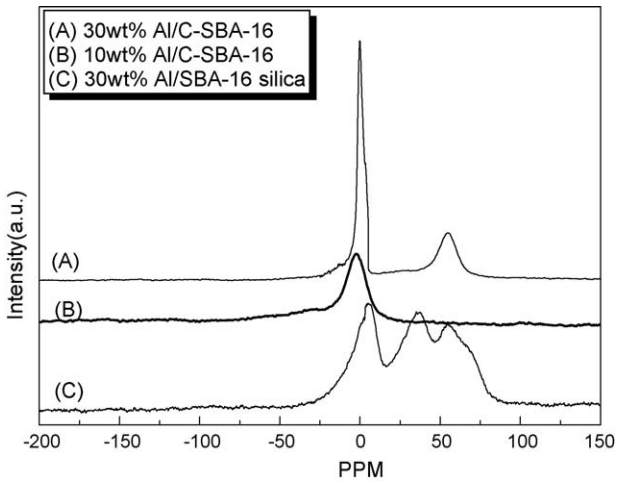

Fig. 7. ^{27}Al-MAS-NMR spectra of 30 wt% $AlCl_3$-loaded C-SBA-16(A); 10% $AlCl_3$-loaded C-SBA-16 (B); 30 wt% $AlCl_3$-loaded SBA-16 silica (C) (samples were calcined at 550 °C in N_2).

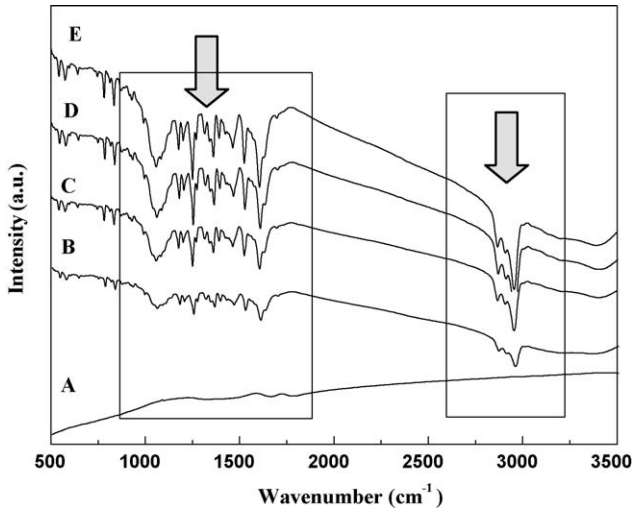

Fig. 8. FT-IR spectra of C-SBA-16 support (A); chiral salen complex immobilized on 10 wt% $AlCl_3$ loading C-SBA-16 (B); chiral salen complex immobilized on 20 wt% $AlCl_3$ loading C-SBA-16 (C); chiral salen immobilized on 30 wt% $AlCl_3$ loading C-SBA-16 (D); and pure chiral homogeneous salen complex (E).

carbons. However, the BrÖnsted acid site itself may result in the fatal drawback of racemization during the asymmetric reactions.

The pure mesoporous carbon, homogeneous chiral Co (III) salen cobalt complexes and those immobilized on the carbon support were characterized by FT-IR analysis (Fig. 8). The mesoporous SBA-15, -16 and the replica carbons can supply the vacant spaces enough to introduce the big salen complexes inside the pore channels. The characteristic peaks for homogeneous chiral cobalt (III) salen complex appeared at the position of 2958–2950, 2912, 1612 and 1535 cm^{-1}, respectively. Those peaks were not found on the IR spectrum of carbon monolith support (Fig. 8A), but the chiral cobalt (III) salen complex immobilized on the meso/macroporous carbon support (Fig. 8B–D) exhibited the similar absorption IR bands as the pure homogeneous cobalt (III) salen complex (Fig. 8E), showing that the salen complex was successfully attached on the surfaces of mesoporous carbon monolith.

3.3. Asymmetric catalysis on heterogenized salen catalysts

To observe the trends in the activity and enantioselectivity of chiral cobalt-salen complexes immobilized on the meso/macroporous carbon C-SBA-16 and silica SBA-16, the reactivities of the homogeneous and heterogenized chiral (salen) Co-BF_3 complexes were examined in the HKR of (±) ECH with a prolonged reaction time. The reaction results are summarized in Fig. 9. The reaction with catalyst 30 wt%-Al/C-SBA-16 led to 99 ee% of ECH after 28 h, and the turn over frequency (TOF) at the initial reaction stage was 6.6 h^{-1}. Whereas 30 wt%-Al/SBA-16 silica catalyst having the similar pore structure gave a lower TOF of 5.0 h^{-1}. The highest TOF of 7.1 h^{-1} was shown for the homogeneous Co-salen catalyst. It is evident that the immobilized Co(III)-BF_3 salen catalyst on the meso/macroporous C-SBA-16 exhibited high activity and selectivity as the homogeneous one. However, with the chiral salen complex over SBA-16 meso/macroporous silica, a lower catalytic activity was obtained even after a prolonged reaction time. This result indicates that the characteristics of the support surface played an important role in the catalysis. The reactant water can be easily adsorbed on the hydrophilic surfaces of silica SBA-16 (or -15) compared to the hydrophobic surfaces of carbon C-SBA-16 (or -15) support, delaying the reactions under the same conditions. The enantioselective ring-opening reaction of epoxides was found to be applicable for the synthesis of an enantiopure terminal epoxide using water as a nucleophile.

As can be seen in Fig. 9, higher reaction rates and ee% of product ECH were observed when the high concentration of active sites (salen complex) was allowed on the same amount of supports with same reaction times. The anchored amount of salen complex was proportional to that of Al present on the supports (EDX result in Fig. 10). The attached contents of Co-salen complex were 4.1, 7.8 and 9.7 wt% over 10, 20 and 30 wt% Al-loaded mesoporous meso/macroporous C-SBA-16, respectively. The remarkable correlation between the reaction rates and the population of salen catalysts on the support was evident from the result of catalysis. When the aluminum chloride content was high, the action of the chiral catalysts became superfluous. This result gives a strong support to a cooperative bimetallic mechanism involving a simultaneous activation of both epoxide and nucleophile by different cobalt-salen units.

The recyclability of catalysts was investigated in HKR of (±) ECH by using different Al-loaded carbon catalysts. The catalyst was collected by simple washing with MC, THF solvent for reuse after completion of reaction. The catalytic activity and enantioselectivity decreased slightly after fourth-time reuse, as shown in Fig. 11. When the catalyst was used without further regeneration, it was

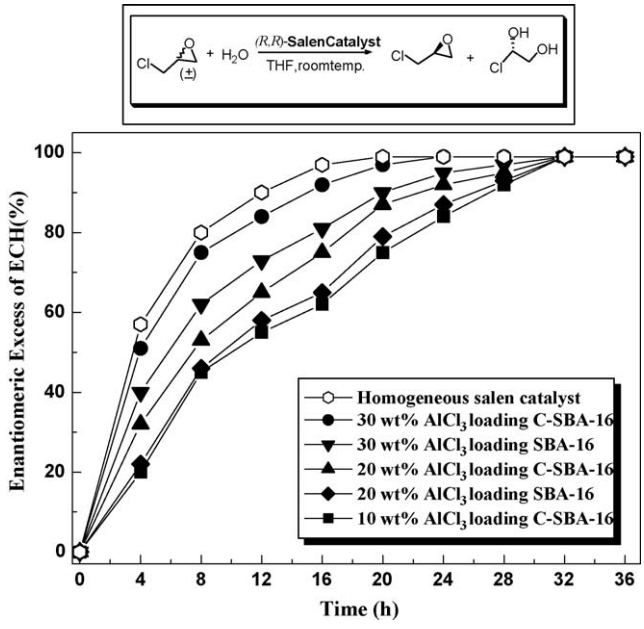

Fig. 9. Effect of loading amount of Al added to the support (SBA-16 carbon and silica monolith) for immobilization of the salen complex on the catalytic activity in HKR of racemate ECH (1.0 mol% salen relative to ECH was loaded in the system).

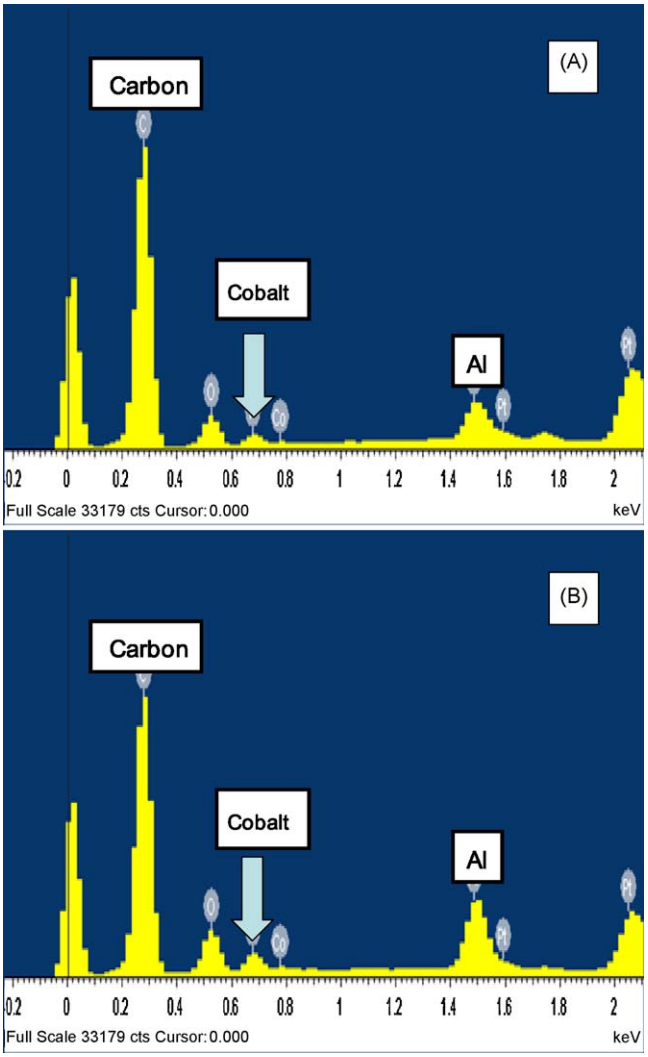

Fig. 10. Energy dispersive X-ray analysis pattern of 10 wt% $AlCl_3$ loading C-SBA-16 (A); 20 wt% $AlCl_3$ loading C-SBA-16 (B).

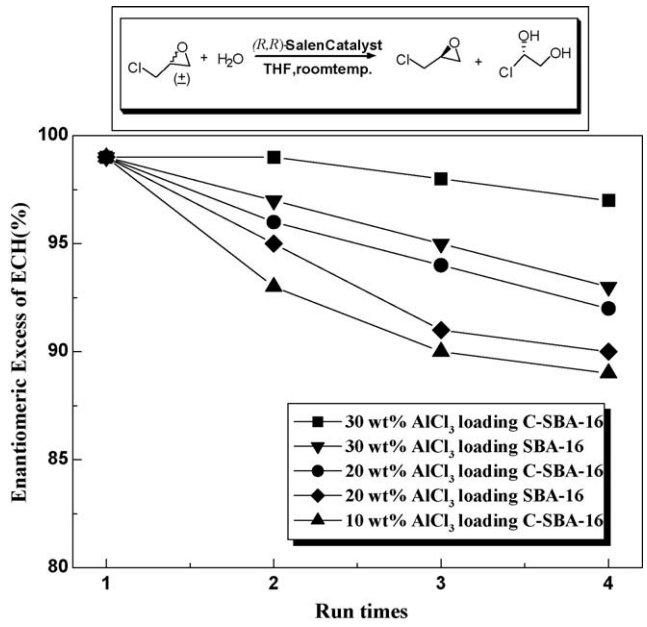

Fig. 11. Recyclability of catalysts in HKR of (±) ECH by using different amounts of Al-loaded SBA-16 carbon and silica monolith catalysts (1.0 mol% salen relative to ECH was loaded in the system. No further regeneration was applied for repeated use).

investigated that a little amount of leaching of homogeneous salen from the support occurred. It is noteworthy that the heterogeneous catalyst could be successfully recycled without much loss in activity after re-attachment of chiral Co(III)-BF_3 salen on the reused catalysts in MC solvent. It was easy to isolate the immobilized salen catalysts from the product solution containing epoxide and diol.

4. Conclusions

The meso/macroporous materials having bimodal pore structures were synthesized, and their pore system was characterized by instrumental analysis and by comparing the catalytic activity at room temperature. Large carbon monoliths could be obtained in centimeter scale from its corresponding template silica monolith. The adjacent macropores are interconnected through uniform-sized windows, and the walls of these macrospheres consist of mesostructured pores. On the basis of asymmetric HKR of ECH with various catalysts, the chiral Co(III)-(BF_3) salen immobilized on the functionalized meso/macroporous carbon monoliths obtained in the present study can be applied as effective heterogenized catalysts for asymmetric reactions. The catalysts were prepared with different loading amounts of aluminum chloride to anchor the active salen complex, and the catalytic activity increased with increasing amount of aluminum chloride on the surfaces. The robust catalytic properties of meso/macroporous carbon materials may expand the applications of porous materials. Furthermore, such carbon materials with bimodal meso/macroscopic pores would be useful for many potential applications, such as heterogeneous catalysts when bulky or highly hydrophilic molecules are involved as a reactant.

References

[1] R. Ryoo, S.H. Joo, S.J. Jun, J. Phys. Chem. B 103 (1999) 7743.
[2] R. Ryoo, S.H. Joo, M. Kruk, M. Jaroniec, Adv. Mater. 13 (2001) 677.
[3] S. Jun, S.H. Joo, R. Ryoo, M. Kruk, M. Jaroniec, Z. Liu, T. Ohsuna, O. Terasaki, J. Am. Chem. Soc. 122 (2000) 10712.
[4] S.H. Joo, S.J. Choi, I. Oh, J. Kwak, Z. Liu, O. Terasaki, R. Ryoo, Nature 412 (2001) 169.
[5] S.S. Kim, T.J. Pinnavaia, Chem. Commun. (2001) 2418.
[6] S.B. Yoon, J.Y. Kim, J.S. Yu, Chem. Commun. (2001) 559.
[7] S.J. Han, T. Hyeon, Chem. Commun. (1999) 1955.
[8] S.J. Han, T. Hyeon, Carbon 37 (1999) 1645.
[9] J. Lee, K. Sohn, T. Hyeon, J. Am. Chem. Soc. 123 (2001) 5146.
[10] J. Lee, K. Sohn, T. Hyeon, Chem. Commun. (2002) 2674.
[11] J. Lee, J. Kim, T. Hyeon, Chem. Commun. (2003) 1138.
[12] H.C. Foley, Microporous Mater. 4 (1995) 407.
[13] T. Kyotani, Carbon 38 (2000) 269.
[14] B.H. Han, W.Z. Zhou, A. Sayari, J. Am. Chem. Soc. 125 (2003) 3444.
[15] H.F. Yang, Q.H. Shi, X.Y. Liu, S.H. Xie, D.C. Jiang, F.Q. Zhang, C.Z. Yu, B. Tu, D.Y. Zhao, Chem. Commun. (2002) 2842.
[16] Y.D. Xia, R. Mokaya, J. Phys. Chem. C 111 (2007) 10035.
[17] A. Taguchi, J.H. Smatt, M. Linden, Adv. Mater. 15 (2003) 1209.
[18] Z.G. Shi, Y.Q. Feng, L. Xu, S.L. Da, M. Zhang, Carbon 41 (2003) 2677.
[19] O. Klepel, H. Straub, A. Garsuch, K. Bohme, Mater. Lett. 61 (2007) 2037.
[20] X.Q. Wang, K.N. Bozhilov, P.Y. Feng, Chem. Mater. 18 (2006) 6373.
[21] S. Alvarez, J. Esquena, C. Solans, A.B. Fuertes, Adv. Eng. Mater. 6 (2004) 897.
[22] S. Alvarez, A.B. Fuertes, Mater. Lett. 61 (2007) 2378.
[23] Y.S. Kim, C.-Y. Lee, G.-J. Kim, Bull. Korean Chem. Soc. 30 (2009) 1771.
[24] IUPAC reporting physisorption data for gas/solid systems with special reference to the determination of surface area and porosity, Pure Appl. Chem. 57 (1985) 603.
[25] J. Gan, T. Wang, Z. Liu, W. Tan, Stud. Surf. Sci. Catal. 170B (2007) 1567.